

# Competing forces of polarization and confinement generate cellular chirality in a minimal model

Egun Im [a]      Ghina Badih [b]      Laetitia Kurzawa [b]      Andreas Buttenschön [c]  
 Calina Copos [a,d]

## Abstract

Left-right axis specification is a vital part of embryonic development that establishes the left and the right sides of an embryo. Asymmetric organ morphogenesis follows asymmetric signaling cascades, which in turn follow asymmetric events on the cellular scale. In a recent study, Badih et al. reported cell-scale movement asymmetries in spontaneously rotating pairs of endothelial cells confined to a circular fibronectin-coated island. Importantly, the authors demonstrate that cytoskeletal contractility modulates the chirality bias. The relative simplicity of the experimental setup make it a perfect testing ground for the physical forces that could endow this system with rotational movement and biases, but these forces have yet to be stated. We model self-propelling biological cells migrating in response to confinement, polarity, and pairwise repulsive forces. For the first time, we are able to reproduce not only the coherent angular movement of a confined pair of cells biased in a direction but also a contractility-modulated chirality bias. To arrive at these modeling results, two key assumptions are needed: an intrinsic orientation bias (previously observed in other cellular systems), and a difference between the cells in their velocity alignment response, which endows the system with a difference in the timescales of dynamics. Tuning the timescale (or strength) of polarity response relative to the remaining forces (confinement and cell-cell interaction), can amplify or reverse the CW bias.

**Significance Statement:** Left-right asymmetry is a vital part of embryonic development and its origins can be traced back to the dynamics of individual cells regulated by mechanical and biochemical signaling cues. Recent experiments showed that cellular movement chirality can be established and lost by varying cellular contractility in a minimal system of a pair of cells confined to a disk geometry. Here, we present a coherent theory identifying how physical forces can distinguish left from right and thus endow a system with a rotational bias. We demonstrate that to recapitulate earlier experimental results with a model, individual cells must have an intrinsic bias. We further find that by tuning the strength of cell contractility, cells tune their adherence to the local environment but also to each other. A tug-of-war emerges between their ability to move directionally, albeit with a slight tilt, and the strength of centering forces from cell-cell and cell-matrix adhesions. This study thus posits a minimal description of the physical forces determining the chiral rotation of small cell collectives.

**Keywords:** left/right asymmetry, chirality, collective cell motility, computational modeling

## I. INTRODUCTION

Chirality, the property of an object that lacks mirror symmetry, is a conserved feature of living organisms with critical implications during embryonic development [35, 21, 10, 12, 39, 2]. For example, in the mouse

embryo, rotating cilia generate a right-to-left fluid flow fundamental to the organism's left-right asymmetry of organ positioning and shape during development [23]. Asymmetric organ morphogenesis is believed to be controlled by differential expression of signaling cascades reviewed in [21] – for example, in both chick and mouse normal embryos, Nodal expression is observed on the left side. There is increasing evidence that these signaling networks in turn must follow asymmetric events by their constituent cells [25, 18]. Beyond biological cells, there is a growing interest in chiral active matter including a variety of biological circle swimmers, such as *E. coli* [4, 13, 11, 20], sperm [26, 16], and magnetotactic bacteria [14, 6], but also synthetic self-propelled chiral particles [31, 7].

One of the main unresolved issues arising in both active and biological matter is the ability to identify the macroscopic forces that distinguish left from right to form and abolish biased movement. Here, we focus on a minimal experimental setup that demonstrates robust control of biased rotational movement of a pair of cells in a confined geometry [3]. A few important observations were made in this minimal system composed of a pair of endothelial cells confined to a disk-shaped fibronectin-coated micropattern (Fig. 1A). (1) The doublets spontaneously and persistently rotate, albeit not always (Fig. 1B). (2) A mild bias towards clockwise rotation was shown (Fig. 1B). The HUVEC doublets illustrate a CW bias with 80% of the cells rotating persistently and of those 60% in the CW-direction on average. (3) The chirality

bias can be amplified or reversed by modulating contractility forces (Fig. 1C). CW doublets rotate faster and exert less forces compared to their CCW counterparts. (4) Using contractility modulating drugs, such as Rho kinase inhibitor (ROCKI) and Calyculin A (CalyA), the bias could be amplified or reversed (Figs. 1D-E). The authors speculate that the speed and direction of rotation are determined by the more contractile cells within the doublets. Even so, a mechanistic understanding of how mechanical forces are integrated to give rise to chiral bias remains unknown. Specifically, no macroscopic force distinguishes left from right, which leaves the question of how does bias emerge? Furthermore, what physical forces does contractility modulate? Is the directionality bias a result of competing force strengths or timescales in the system?

Previous models of rotations of cell groups have been proposed, some of which explicitly capture biases [15, 34, 37, 29] while others do not [33, 32]. In particular, the actin network integrity and actin-related proteins have been implicated in the establishment of the chirality of movement including formins [30], alpha-actinin [28, 36, 8], myosin [36], and associated signaling pathways [15]. None of these theoretical works focus on the modulation of chirality. We address this critical question in this work.

We begin with a focus on recent experiments performed in [3]. Using analytical and computational tools applied to a mathematical model, we recreate these experiments to examine the rotational movement patterns of a pair of cells confined to a disk geometry. Using a friction-dominated minimal system, we can recapitulate unbiased rotational movement in this confined geometry, but also the emergence of CW or CCW biased movement depending on the relative strengths and timescales of spontaneous polarization and cell-cell or cell-matrix adhesions. Modulating polarity response, which in our model is related to the cellular contractility, can amplify or reverse the chirality bias just as observed experimentally. Through linear stability analysis, we determine the parameter space of possible behaviors. Our study, therefore, provides a minimal description of the macroscopic cellular forces that produce bias.

## II. MATHEMATICAL MODEL

We build a minimal mathematical model to capture the interplay between cell polarity, contractility, and spatial confinement. For simplicity, we first describe the model for a single-cell system confined to a disk-shaped adherent micropattern (Fig. 2), the same geometric confinement as in [3]. In our model, the cell is represented by the position of its center-of-mass and further detailed morphology such as cell membrane, nucleus, or actomyosin cytoskeleton are ignored. Taking the overdamped (or viscous dominated) approximation to a physical system

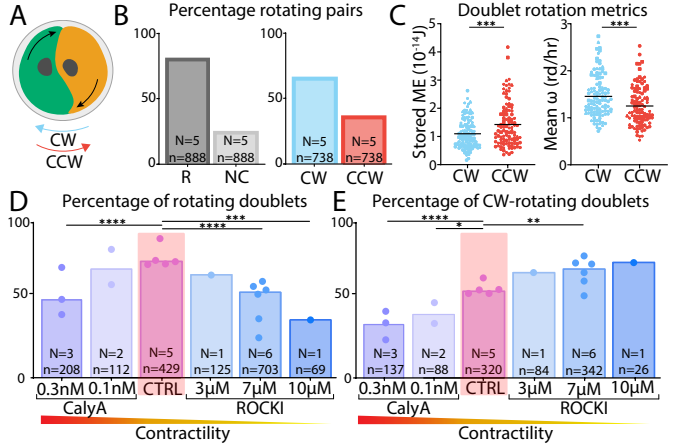


**Figure 1: Summary of experimental results of Badih et al. on the movement of HUVEC pairs confined to a disk-shaped geometry.** (a) Schematic of the experimental setup illustrating two HUVEC cells confined to a disk-shaped adherent geometry with  $R = 60 \mu\text{m}$ . (b) Summary of experimental results illustrating a three-state migratory system: doublets rotating coherently (R) in either the clockwise (CW) or counterclockwise (CCW) direction or switching direction of rotation (NC). (c) The doublets are characterized by an asymmetry in the stored mechanical energy as reported by traction force measurements and in the angular speed; Statistical significance was assessed using an unpaired t-test ( $p = 0.0087$  for left plot;  $p = 0.0110$  for right plot).  $N = 3$  independent experiments, and  $n = 98$  doublets for both plots. (d) Percentage of rotational doublets and (e) percentage of CW-rotational doublets, both showing directional biases modulated by contractility. Quantified in control versus treated, from decreasing concentrations of CalyA to increasing concentrations of ROCKI. Statistical significance was assessed using Chi-squared test (Fischer's exact; Significance testing: \* = 0.01238; \*\* = 0.0087; \*\*\* = 0.0007; \*\*\*\* < 0.0001).  $N$  indicates the number of individual experiments and  $n$  the total number of doublets used for quantification.

— a point at location  $\mathbf{x}(t)$  moves with velocity  $\mathbf{v}(t)$  according to its local force balance:

$$\sum \mathbf{f}(\mathbf{x}(t), t) = 0 \Rightarrow \mathbf{v} = \dot{\mathbf{x}} = \frac{1}{\xi} (\mathbf{f}_{\text{polarity}}), \quad (1)$$

where  $\xi$  is the viscous drag coefficient, effectively equivalent to elastic cell-matrix interactions under conditions of high dissociation rates of these adhesion bonds [17]. The forces per unit length acting on the point are: (1) frictional drag force between the cell and the surface underneath ( $\mathbf{f}_{\text{drag}} = \xi \dot{\mathbf{x}}$ ), and (2) active polarity force arising from front-rear signaling of actin-based protrusion and myosin-based contraction ( $\mathbf{f}_{\text{polarity}}$ ).

**Cell polarity.** Migrating cells have an underlying chemical polarization, indicating the areas of the cell that are

likely to protrude (“front-like”) and those likely to contract (“rear-like”) [19]. This can include asymmetric distribution of Rho GTPases, with Rac1 activity driving the cell front through lamellipodial extensions, and RhoA promoting myosin contractility in the rear. Rather than explicitly modeling the dynamics of one or more Rho GTPases [24, 1, 9], we summarize cell polarity with a single spatiotemporal motility force  $\mathbf{f}_{\text{polarity}}$ . This force is a vector with direction  $\phi$ , initially chosen randomly, and magnitude  $\gamma_{\text{pol}}$  a model parameter:

$$\mathbf{f}_{\text{polarity}} = \gamma_{\text{pol}} (\cos \phi, \sin \phi)^T, \quad (2)$$

and over time evolves via the mechanism of velocity alignment [5]:

$$\dot{\phi} = \frac{1}{\tau_{\text{VA}}} \arcsin [\cos \phi \sin \theta_V - \sin \phi \cos \theta_V]. \quad (3)$$

Here,  $\theta_V$  is the angle of the polar parameterization of the velocity vector  $\mathbf{v}$  and computed every time step as  $\arctan(v_y/v_x)$ , and  $\tau_{\text{VA}}$  sets the orientational persistence timescale. A long timescale,  $\tau_{\text{VA}} \gg 1$ , would imply the cell’s orientation is insensitive to its own velocity direction (Fig. 3H). This form is the one suggested originally by [27] and later adapted by [5] and others.

**Spatial confinement.** To ensure that the cell remains geometrically constrained to the fibronectin-coated micropattern of radius  $R$ , we incorporate confinement through a reorientation of the polarity angle in Eq. 3:

$$\begin{aligned} \dot{\phi} &= \frac{1}{\tau_{\text{VA}}} \arcsin [\cos \phi \sin \theta_V - \sin \phi \cos \theta_V] \\ &\quad + \frac{1}{\tau_W} \arcsin [\cos \phi \sin \theta_W - \sin \phi \cos \theta_W], \end{aligned} \quad (4)$$

where  $\theta_W$  is the angle pointing from the cell’s position toward the center of domain. This implicit formulation captures how cells with finite spatial extent continuously sense the domain boundaries through their cytoskeleton. Since the polarization represents an averaged cytoskeletal response, the reorientation mechanism naturally accounts for the cell’s distributed sensing of geometric constraints without requiring an artificial radial potential that switches on and off at a specific threshold. In the absence of such a confinement effect, the cells engage in persistent directional motion (Fig. 3D). We find that this implicit approach successfully recapitulates the experimental findings.

### III. RESULTS

#### A. Model predicts three-state dynamics of single cell movement on circular micropatterns

To probe the single-cell system response, we placed a cell in the center of the disk-shaped micropattern, induced

the cell polarization in a random direction, and let the system evolve according to Eqs. 1, 2, and 4 for 2 hrs (Fig. 2A). Fig. 2B plots one rotational cycle, in either direction, as the singlet navigates the confining geometry in our simulation. Along with trajectories, we plot the angular speed for several initializations and the averaged behavior over 3,200 simulations <sup>1</sup>(Fig. 2C).

Cells display a variety of motility patterns, including cells moving persistently in one direction, either clockwise (CW) or counterclockwise (CCW) (Fig. 2C, Movie 1), or switching direction (Fig. 2C, Movie 2), thus not moving coherently (NC). The marginal case of non-coherent movement appears at very low frequency. To classify the emergent behavior, the time evolution of the angular speed is used – non-coherent movement if the cell switches directionality over some arbitrary percentage <sup>2</sup>, clockwise for negative angular speeds, or counterclockwise otherwise. This means that our model, at its default parameters, predicts three-state behavior with nearly all cells persistently rotating either clockwise or counterclockwise with equal transition rates (Fig. 2D).

To verify the numerical simulation results, we transform to polar coordinates where  $\mathbf{x} = R (\cos \theta \quad \sin \theta)^T$  and introduce the phase-lag  $\Delta\phi = \phi - \theta$ , quantifying the angular offset between cellular polarization and positional angle. Phase-plane analysis in the  $(R, \theta)$  coordinate system reveals two center equilibria located at  $\Delta\phi = \pm\pi/2$  (Fig. 3A). These centers organize the phase-space into distinct dynamical regimes: closed periodic orbits surrounding  $\Delta\phi = \pi/2$  correspond to persistent CCW rotation, while those around  $\Delta\phi = -\pi/2$  yield CW rotation. The invariant manifolds along  $\Delta\phi = 0$  and  $\Delta\phi = \pm\pi$  constitute separatrices partitioning phase-space into equal basin of attractions. Latin hypercube sampling across the phase plane confirms this equipartition, with initial conditions yielding precisely 50% CW and 50% CCW trajectories (Fig. 3B-C).

We wondered what is the smallest perturbation to the single-cell system that could lead to rotational movement bias. We extend the model in Eq. 4 by adding a randomly fluctuating intrinsic bias via the term  $\mu\mathcal{N}(0, 1)$  in the velocity alignment:

<sup>1</sup>Without making assumptions about the underlying ratio of a binary proportion ( $p = 0.5$ ), and assuming a margin of error  $E = \pm 3\%$ , we require  $n = (Z^2 \times p \times (1-p))/E^2 = 1,068$  samples for 95% confidence ( $Z = 1.96$ ). Assuming that the lowest ratio of rotation to non-coherent movement never goes below 30%, we conclude that 3,200 samples yields a 95% confidence with error intervals of  $\pm 3\%$ . Any cases where the ratio of rotation to non-coherent movement falls below 40% will be classified as statistically unreliable.

<sup>2</sup>Over 20% unidirectional for coherent rotation, see SI Table.

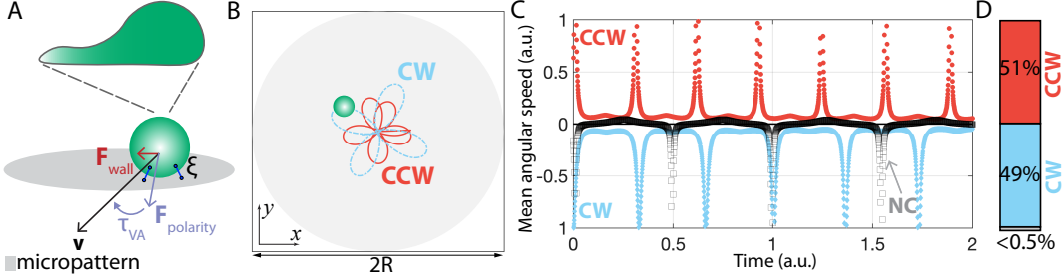


**Figure 2: Schematic representation of the single cell model and resulting behavior.** (A) Singlet model schematic. (B) Sample CW and CCW trajectories over one rotational cycle. (C) Angular velocity over 2 arbitrary time units for cells that move non-coherently by switching directionality (black squares), rotate CW (blue) and CCW (red). (D) Averaged number of rotating doublets and their distribution into the three states: CCW (51%), CW (49%), and NC (< 0.5%) out of 3200 model simulations.

$$\dot{\phi} = \frac{1}{\tau_{VA}} \left[ \arcsin(\cos \phi \sin \theta_V - \sin \phi \cos \theta_V) + \mu \mathcal{N}(0, 1) \right] + \frac{1}{\tau_W} \arcsin(\cos \phi \sin \theta_W - \sin \phi \cos \theta_W). \quad (5)$$

This is our core assumption about how a preferential cellular organization of the cytoskeletal components manifests swirling of the cell body. Our motivation for this is based on the mounting evidence of molecular swirling in the orientation of the cytoskeletal components of some adherent cells [29, 22, 38]. Choosing  $\mu < 0$  sets a clockwise rotation, while a counterclockwise rotation is achieved with  $\mu > 0$ . Bias in either direction led to a tug-of-war between the skewed polarity force and the neutralizing effect of the confinement force (Fig. S1) In the case of  $\mu < 0$ , a CW bias, this intrinsic bias can translate into a bias towards CW rotational movement (Fig. 3E-F). Nontrivially, the skewness in the directionality of the polarity angle also changed the likelihood of observing coherent rotations – lengthening the velocity alignment timescale desensitized the cell to its own intrinsic bias as the symmetric contribution from confinement became dominant (Fig. 3G). A fast velocity alignment timescale (compared to confinement) allowed the cell to re-polarize in the direction of its own velocity, and thus maintain its slight CW bias. However, this ability to re-orient quickly has its downsides – persistent unidirectionality is occasionally lost as evidenced by the increase in noncoherent movement occurrences.

Stability analysis confirms the computational simulations and characterizes the system’s equilibrium structure across parameter regimes. Analytical treatment of the singlet dynamics reveals saddle-center bifurcations at  $\mu = \pm 1$ . For  $|\mu| < 1$ , the system exhibits two coexisting rotational modes with center equilibria at  $\Delta\phi = \pm\pi/2$ . At  $\mu = 0$ , perfect symmetry yields equiprobable CW and CCW rotation with no non-coherent trajectories — all solutions remain confined to their respective basins by the invariant manifolds at  $\Delta\phi = 0$  and  $\Delta\phi = \pm\pi$ . For

$\mu \neq 0$ , the symmetry breaks: negative  $\mu$  biases toward CW rotation while positive  $\mu$  favors CCW, and critically, non-coherent (NC) trajectories emerge as the formerly invariant manifolds become permeable, allowing solutions to transition between rotational domains. Beyond bifurcation points ( $|\mu| > 1$ ), one center annihilates through collision with a boundary saddle, leaving a single dominant rotational mode: CCW for  $\mu > 1$ , CW for  $\mu < -1$ . The Sundman transform and compactification enable complete characterization of the global phase portrait, including heteroclinic connections along invariant manifolds. These results establish that intrinsic polarization bias ( $\mu \neq 0$ ) is both necessary and sufficient to generate directional preference in singlet rotation — without this bias, the system remains perfectly symmetric with equal CW/CCW probability. This fundamental requirement for symmetry-breaking at the single-cell level raises the question: what additional mechanisms beyond intrinsic bias are required to recapitulate the more complex collective behaviors observed in doublet systems in [3].

## B. In the doublet system, model parameter variations alone cannot produce rotational bias

Can our proposed model, extended to cell pairs, simultaneously capture the three-state behavior and a CW bias, as observed for endothelial pairs on adhesive disks in [3]?

To extend our model to multiple cells (Fig. 4A), a cell-cell interaction must be specified. Several possibilities exist, including passive interactions, contact inhibition of locomotion, contact following of locomotion, or more complicated schemes that could involve migration reorientation in response to neighbors’ positions. Here, the intracellular coupling is simply a volume exclusion:

$$\mathbf{f}_{\text{cell-cell}}^{(i)} = k (\|\mathbf{x}_{ij}\| - \ell_0)^- \frac{\mathbf{x}_{ij}}{\|\mathbf{x}_{ij}\|} \quad (6)$$

where  $\mathbf{x}_{ij} = \|\mathbf{x}^{(i)} - \mathbf{x}^{(j)}\|$ , and where  $(f(x))^- = \min(0, f(x))$ . The cell-cell interaction is symmetric but

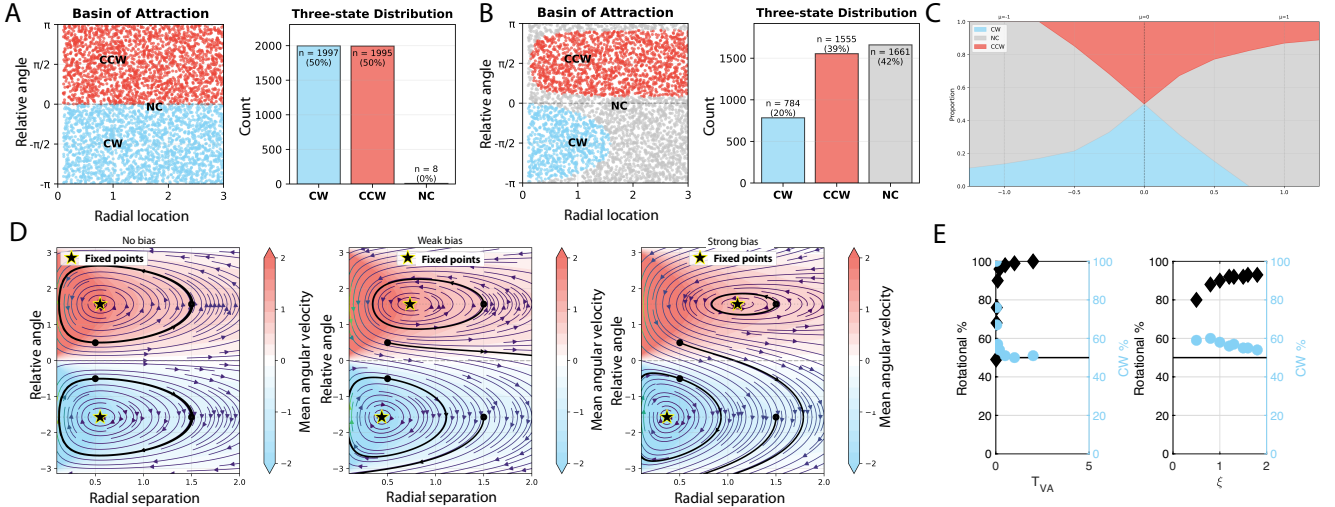


**Figure 3: Under the assumption of intrinsic bias, directionality bias in movement can either be preserved or lost as individual cells explore their confining disk-shaped geometry.** (A) Phase-space analysis without intrinsic bias ( $\mu = 0$ ): Latin hypercube sampling of initial conditions colored by observed angular velocity (left) and histogram of rotational outcomes (right) showing equal 50/50 CW/CCW distribution. (B) Phase-space analysis with intrinsic CW bias ( $\mu < 0$ ): sampled initial conditions colored by angular velocity (left) and histogram (right) revealing broken symmetry with directional preference and emergence of non-coherent (NC) trajectories. (C) Bifurcation diagram scanning intrinsic bias parameter  $\mu$  from  $-1.25$  to  $1.25$ , showing the breakdown of rotational states (CW, CCW, NC) as a function of bias strength, confirming the saddle-center bifurcations at  $\mu = \pm 1$ . (D) Phase-plane portraits illustrating the dynamical system structure for three regimes: no bias ( $\mu = 0$ ), weak bias, and strong bias, showing the evolution of center equilibria and separatrices. (E) Parameter sweep showing the percentage of rotating cells and their orientation distribution as functions of polarization velocity alignment timescale ( $\tau_{VA}$ ) and frictional drag coefficient ( $\xi$ ), demonstrating how the tug-of-war between polarization and confinement modulates directional bias.

opposite, meaning  $\mathbf{f}_{\text{cell-cell}}^{(i)} = -\mathbf{f}_{\text{cell-cell}}^{(j)}$ . The equations of motion for the cell pair confined to the disk are:

$$\sum \mathbf{f}(\mathbf{x}, t) = 0 \Rightarrow \dot{\mathbf{x}}^{(i)} = \frac{1}{\zeta^{(i)}} \left( \mathbf{f}_{\text{polarity}}^{(i)} + \gamma_{cc} \mathbf{f}_{\text{cell-cell}}^{(i)} \right),$$

where  $\gamma_{cc}$  is the symmetric strength of the cell-cell coupling, while  $\mathbf{f}_{\text{polarity}}^{(i)}$  is the polarity force as described in Eq. 2. To preserve generality, we permit heterogeneity between the doublets with different constants for the frictional drag coefficient and relative force strengths.

Fig. 4B plots sample movement trajectories of the cells in the doublet as they navigate the disk-shaped micropattern in our simulation. To assess directionality, the angular speed of the cell-cell separation plane is used with the same criterion as in the singlet case. The cell-cell separation plane is defined to be the line perpendicular to the axis of the radial separation between the cells. We plot angular speed of the cell-cell separation plane for several sample trajectories (Fig. 4C) and the averaged behavior over 3,200 simulations (Fig. 4D). Similar to singlets, the pairs can also either rotate persistently in either the CW or CCW direction (Fig. 4C, Movie 3), or switch direction of rotation, thus not move coherently (Fig. 4C, Movie 4). Similar to the unbiased singlet findings, the marginal case of noncoherent locomotion (NC)

appears in low frequency. All of these behaviors – non-coherent, persistent CW and CCW rotational movement – were observed in the experiments of Badih et al. [3]. When we combine all 3,200 simulations, we find that almost all doublets rotate (95%) with no preferred direction, as indicated by the nearly even distribution between clockwise (~51-54%) and counterclockwise (~46-49%) direction (Fig. 4D). At its default parameters, our model predicts three-state behavior with the majority of cells persistently rotating either clockwise or counterclockwise with equal transition rates. This is contrary to what was observed in the experimental system in [3], where the CW-bias reached about 60% of the rotating doublets.

Forgoing the assumption of intrinsic cellular bias, we wondered if parameter variations could give rise to an asymmetry in the system. We probed whether that was the case with changes in the active force strength ( $\gamma_{\text{pol}}$ ), frictional drag coefficient ( $\xi$ ), response of the velocity alignment mechanism ( $\tau_{VA}$ ), or strength of cell-cell adhesion ( $\gamma_{\text{cell-cell}}$ ). Some of the variations in the parameters did impact the likeliness to rotate persistently – for example, intuitively, simulated cells were more likely to get stuck or switch direction of movement with decreases in the strength of active forces. However, we

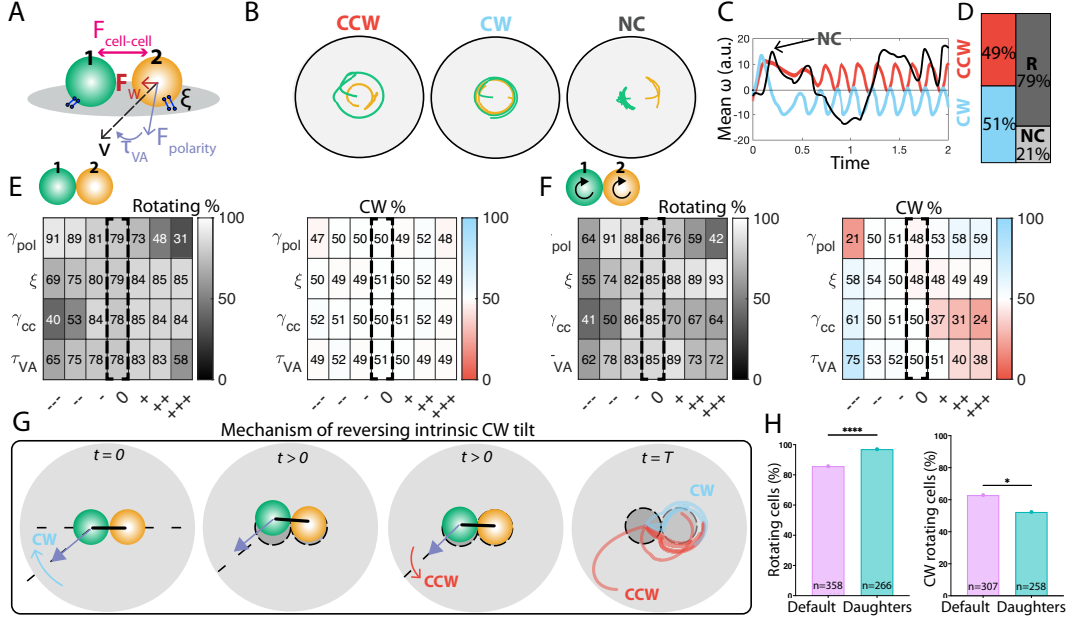


**Figure 4: Intrinsic cellular directionality tilt allows for the emergence of bias in the doublet system.** (A) Doublet model schematic. Emergence of CW/CCW/NC rotational movement: (B) sample simulated trajectories, (C) angular speed over time of the cell-cell separation plane. (D) Summary of the averaged model results for coherent (R) vs noncoherent (NC) rotational movement and split of the rotating cases into CW and CCW directional in the case of (i) no intrinsic cellular bias, (ii) no intrinsic bias with heterogeneity (across all sampled parameters), and (iii) intrinsic bias and frictional drag heterogeneity. Model outcomes for parameter sweeps for doublets (E) without and (F) with intrinsic tilt in the CW direction. Dashed black region indicates homogeneity across the pair and purple dashed region marks 2 or more parameter sweeps with elevated CW bias. (G) Schematic of the ‘tilting dumbbell’ mechanism for reversing the CW intrinsic tilt to a CCW doublet bias. (H) Experimental results for daughter cell pairs. Statistical significance was assessed using an unpaired student’s t-test (\* indicates  $p < 0.01$ , \*\*\*\* indicates  $p < 0.0001$ ).

did not observe a robust bias in any of the cases explored (Fig. 4E). Cell-to-cell variability in the same parameters also had negligible effects (Fig. S2), indifferent of whether the changes were implemented in cell 1 or 2. This told us that neither mechanical or biochemical changes nor heterogeneity alone can account for biases in the system.

### C. Intrinsic bias reveals directionality-tunable rotational movement of doublets

Following the singlet analysis and computational findings that suggested a more responsive polarity machinery (either via strength of active forces or velocity alignment timescale) can yield a robust bias, we similarly introduce a mild CW cellular bias in each cell via  $\mu < 0$  in Eq. 4. This choice is equivalent to a standard uniform distribution with mean < 9 degrees and standard deviation of < 0.1. Indeed, we found that was the case in the doublets (Fig. 4F) – the modification revealed a tug-of-war between the effect of centering mechanical forces (confinement and intracellular coupling) and the biased active force (biochemical polarization). The parameter changes that produced CW bias (blue, Fig. 4F) include

increased strength of active forces, faster velocity alignment response, or weaker frictional drag and cell-cell volume exclusion. Our interpretation is that CW bias emerges when cells behaved more individualistic and/or have a stronger (faster) response in their polarization machinery (which is endowed with a mild intrinsic CW bias in the model). Unlike the singlet results, a CCW bias in rotational movement can also be produced. This happened with decreased strength of active forces, slower velocity alignment response, or stronger cell-cell volume exclusion.

While multiple parameter changes could account for the 60% CW bias observed in the (control) endothelial doublet system, there are two primary reasons we do not consider this perturbation. (1) The cases with CW bias, also correspond to cases where persistence of unidirectional rotational motion is diminished significantly ( $\leq 65\%$ ) – which is not in agreement with experimental findings (Fig. 1B). (2) Moreover, these parameter variations are done simultaneously across both cells, yet in [3], it was suggested that there is a mechanochemical asymmetry between the cells (Fig. 1C, Fig. 4B in [3]). Inspired by Badih et al.’s measurements of statistically significant

differences in the exerted mechanical energy, we posited that cell-to-cell differences could give rise to a chiral bias.

Indeed, that was the case – setting an asymmetry in the velocity alignment timescale (in either cell) produced a modest reduction in the number of rotating doublets from 85% to 71%, with 61% of those persistently rotating doublets in CW arrangement (purple regions, Fig. 5A-C). Recapitulating the experiments was also the trend in the rotational speed – CCW doublets have a significantly lower angular speed compared to CW doublets (Fig. 5D). Our explanation for the reduction in number of rotating doublets is the number of collisions increases once an asymmetry in timescales is introduced. The combination of centering forces from confinement and volume exclusion, ensures that the system moves as a dumbbell with an end that is more responsive to its CW-biased polarity machinery.

Qualitatively the same trends observed with homogeneous variations in frictional drag coefficients and polarity strength (Fig. 4F) continued in the heterogeneous cases (Fig. 5A-B). Frictional drag alone had negligible effects on the percentage of CW rotating doublets, and changes in the polarity strength could only produce more CCW pairs. The model informed us that even though the observable differences are in the stored mechanical energy of the doublets, the dominating effect is in the timescale of response of the polarity machinery. In other words, a more contractile cell has a more responsive velocity alignment mechanism and is able to orient its motility direction along the Rac/Rho polarity axis.

#### D. Daughter pairs lack mechanical heterogeneity and exhibit no rotational bias

The model makes two predictions. (1) There is an intrinsic cellular bias (assumed, rather than explicitly captured in our model). (2) By default, cells are primed along the unbiased parameter regime, and additional changes via either drug perturbations or cell-to-cell variability lead to a rotational bias. If we start under the assumption of parameters along the bifurcation line, our model postulates that if there are no additional differences between the cells in terms of their contractility (and therefore, their cell-matrix drag coefficients), the cells rotate persistently in either direction (dashed region, Fig. 5A). To test whether this modeling prediction has any grounding in the biological setting, we examined the response of a pair of daughter HUVEC cells in the same  $60 \mu\text{m}$  disk-shaped micropattern as in [3]. We found that our modeling prediction that heterogeneity underpins the emergence of bias was indeed recapitulated in the experiments with daughter doublets (Fig. 4H).

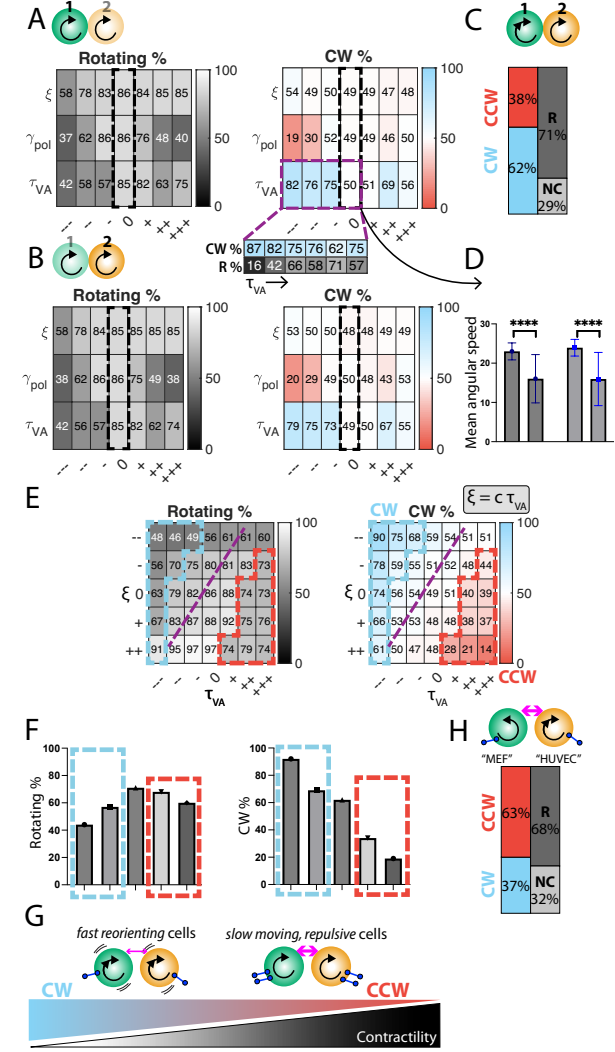


**Figure 5: Chirality bias is modulated by an interplay between strength of confinement, polarity, and cell-cell coupling forces.** CW bias emerges in the presence of velocity alignment heterogeneity, and be amplified with faster polarization timescales. A slower polarization response together with dominating allows for the emergence of CCW bias can be achieved through dominating contact inhibition of locomotion. (A), (C)-(E) Parameter sweeps for various considerations. For the case of passive elastic bonds for the cell-cell interactions and frictional asymmetry in the doublets, two separate parameter sweeps were performed across other heterogeneity in either (A) the ‘sticky’ cell or (C) the motile cell. (B) Angular speed for CW and CCW rotating doublets across the purple region in the adjacent subplot. For the case of CIL-like cell-cell interactions, we considered parameter variations for (D) the frictional asymmetry scenario separately from (E) the homogeneous scenario. Dashed black region indicates homogeneity across the pair and purple dashed region marks 2 or more parameter sweeps with elevated CW (or CCW) bias. (F) Schematic of working hypotheses with contractility modulation.

### E. Differences in frictional drag, polarity, and cell-cell adhesion parameters strengthen or reversed the CW rotational bias of doublets

Having established that an intrinsic CW bias together with cell-to-cell heterogeneity in the velocity alignment response can yield the default doublet case (Fig. 5C), we next wondered what is modulated by the contractility inhibitors to further increase the CW bias of the system.

To illustrate the model outcome, we focus on two parameter variations –  $\xi$  tunes the strength of the frictional drag and  $\tau_{VA}$  tunes the timescale of velocity alignment in the polarity force (Fig. 5E). Mathematically, we discovered an effective bifurcation line  $\xi = c\tau_{VA}$  where CW bias emerges for  $c > c_{crit}$  and a CCW bias otherwise. Here,  $c_{crit}$  marks the point where no bias is expected. By tuning model parameters respective to this bifurcation line, in a way that we will demonstrate is congruent with the experimental perturbations of cellular contractility, we were able to reproduce motility biases similar to those observed experimentally (Fig. 5F).

If the polarity response dominates (top left, Fig. 5E), then the doublets' motility is dominated by their intrinsic CW bias and the overall doublet motility has a CW bias. For a fixed parameter choice ( $\xi = \xi_0$ ), decreasing the velocity alignment response timescale produced a reduction in the number of rotating doublets from 86% to 63%, with 74% of those persistently rotating doublets in CW arrangement (blue region, Fig. 5E). Otherwise, if the polarity response was longer, counterintuitively a CCW bias emerges (bottom right, Fig. 5E). The biases are augmented with changes in the drag coefficient – 90% of rotating doublets orient in the CW direction with a fast re-orientation timescale and fast motility, whereas only 14% of doublets rotate in the CW direction with a slow re-orientation timescale and slow motility dynamics. Based on these insights into how these two model parameter variations mold the doublet behavior, we explain how the rotational bias is strengthened and reversed by the contractility perturbations in Fig. 1D-E.

Badih et al. reported that when doublets were treated with a Rho kinase inhibitor, the system exhibited a more pronounced asymmetry in the CW direction with an overall lower percentage of persistently rotating doublets (Fig. 1D-E). Based on the parameter variations in Fig. 5E, we posited that ROCK inhibitors increase the cell polarity response and decrease the frictional drag. Indeed, we found that to be the case in a gradual (titratable) manner – when the velocity alignment timescale is gradually reduced (while maintaining the initial cell-to-cell asymmetry), CW bias is increasingly produced while the number of rotating cells decreases (left, Fig. 5F). A similar response can be attained by increasing the polarity strength coefficient,  $\gamma_{pol}$ , while simultaneously decreasing frictional drag coefficient (Fig. S3). While weakening the strength of cell-cell interactions did also

lead to more CW rotating cells, we found that it also increased the number of rotating pairs which was not observed experimentally. Coupling the increase in polarity strength with weaker cell-cell adhesion did recover the pronounced CW bias in a diminishing number of rotating pairs (Fig. S4). Taken together, these results suggested to us that the addition of the ROCK inhibitor, activated the polarization machinery relative to other physical forces in the system (cell-cell interactions or confinement).

What about the control mechanism for flipping the skewness of the rotational orientation towards the CCW direction? The experiments of Badih et al. found that Calyculin A, which enhances cellular contractility through increased phosphorylation of myosin light chain, increased the stored mechanical energy of the doublets. More surprisingly, it flipped the prior observed CW-bias in coherent rotations while simultaneously lowering the likelihood of engaging in coherent rotational movement (Fig. 1D-E). We interpreted increased contractility in the model by making two key assumptions – the velocity alignment timescale is longer, and the frictional drag coefficient is higher (bottom right, Fig. 5E). Our rationale is that more contractile cells are more adherent and, thus, have slower dynamics of polarization and motility. Importantly, we found that if we maintained the assumption of cell-to-cell asymmetry in the polarity timescale, we needed to increase the volume repulsion strength to decrease the percentage of coherent rotation. This assumption is also experimentally motivated – in the Calyculin A experiments, the nuclei appear to be further apart suggestive of a result due to repulsive rather than attractive interactions such as those of a passive adhesion. In this scenario, with the same assumptions of CW intrinsic bias in each cell, led predominantly, to CCW rotations (Fig. 5F). We found that simultaneously increasing the drag and velocity alignment timescale coefficients led increasingly to fewer coherently rotating doublets, yet of those rotating doublets, more CCW bias. This led us to conclude that the Calyculin A treatment diminished the contribution of the CW biased intrinsic polarity machinery in exchange for stronger repulsive interactions between the cells.

### F. In the model, the timescale of the response of velocity alignment governs the directionality of the rotational bias

In our mathematical model, we found that frictional drag together with cell polarity response (strength or velocity alignment timescale) to be a proxy for cellular contractility. As a last test of this modeling framework, we wondered if we could replicate the heterotypic doublet experiments in Badih et al. The authors showed that a doublet system composed of a contractile MEF together with an HUVEC exhibited not only a high difference in contractility but also a clear CCW rotational bias. Im-

portant for our model assumptions, the MEF cells have a very different population bias – at the population level, MEF cell clusters tilt in the CCW orientation, oppositely of the HUVEC clusters. To test our model predictions, we coupled our default HUVEC-like cell to a cell with an opposite (CCW) intrinsic bias ( $\mu > 0$ ) in the same disk-shaped geometry. Not surprisingly, given that all other parameters are the same across the cells, we found no emergent bias – 81% of doublets rotate coherently and 50% of those are in the CCW direction (Fig. 5G). But if we further enforce that MEF cells have a longer velocity alignment response (the same assumption as our more contractile manipulation in Section E), we find that the doublet system rotates with a smaller percentage coherently (70%) but of those cases, 60% are in the CCW direction (Fig. 5G). We note that to obtain these results, we found that yet again we need to increase the strength of cell-cell repulsion and that a two-fold higher value for the velocity alignment timescale is needed to reproduce the observations. Further increasing the velocity alignment timescale yields even more CCW bias and fewer rotating cells. Importantly, we find that the directionality of the intrinsic bias plays no role and same can be said of the friction coefficient (neglected in this heterotypic-like case). In regards to the directionality of the intrinsic bias, we intuit that the bias serves as a perturbation rather than a driver of the underlying dynamical system, as described in Section A and Fig. 3.

#### IV. DISCUSSION

Our model constitutes a minimal biophysical framework that identifies the physical requirements for directional asymmetry in the motility of a two-cell system confined to a disk geometry. To recapitulate the experimentally observed rotational directional bias in HUVEC doublets [3], two critical ingredients are required: (1) individual cells must possess an intrinsic directional bias, and (2) mechanical heterogeneity between the cells, specifically asymmetry in the velocity alignment response timescale  $\tau_{VA}$  that governs how quickly cells reorient their polarity in response to their own velocity. These two assumptions together create a tunable tug-of-war between biased polarization forces and symmetric centering forces from confinement and cell-cell interactions. By modulating the relative strengths and timescales of these competing forces — which we interpret as changes in cellular contractility — the system can amplify or reverse its rotational bias, precisely as observed experimentally with ROCK inhibition and Calyculin A treatment.

Phase-plane analysis of the singlet system establishes the fundamental dynamical structure underlying chiral rotation. The analysis of the singlet system reveals two center equilibria one for CW and CCW rotation. Without intrinsic bias ( $\mu = 0$ ), equal basins of attraction yield 50/50 CW/CCW probability. Intrinsic bias ( $\mu \neq 0$ )

breaks symmetry and enables non-coherent (NC) trajectories. Crucially, bias expression depends on timescales: fast velocity alignment preserves CW bias, slow alignment lets confinement dominate and erase it. Intrinsic bias is necessary but not sufficient for directional bias.

Extending the model to doublets introduces a fundamentally new force: cell-cell mechanical coupling through volume exclusion. This repulsive interaction, symmetric but opposite between cells, activates when cells approach within a critical distance, creating sporadic but strong mechanical constraints. The doublet system now balances three competing forces: two independent polarization forces (one per cell), symmetric confinement from the boundary, and pairwise repulsion. This additional mechanical coupling fundamentally alters the dynamics compared to isolated singlets, raising the question of whether cell-cell interactions alone can generate rotational bias.

We first tested whether doublets with symmetric parameters could produce rotational bias. Parameter variations in  $\gamma_{pol}$ ,  $\xi$ ,  $\tau_{VA}$ , or  $\gamma_{cc}$  alone — without intrinsic bias — maintain 50/50 CW/CCW split (Fig. 4E). This demonstrates that mechanical or biochemical changes alone, when cells remain homogeneous, cannot break rotational symmetry. An asymmetry-breaking mechanism is required.

Introducing intrinsic CW bias ( $\mu < 0$ ) in both cells breaks the symmetry. With homogeneous parameters, some directional preference emerges, but the bias is weak and depends sensitively on parameters choices (Fig. 4F). However, when we additionally introduce heterogeneity — specifically difference in velocity alignment timescales ( $\tau_{VA}^{(1)} \neq \tau_{VA}^{(2)}$ ) between cells, representing differences in how quickly cells reorient their polarity — robust and tunable bias emerges. Parameter sweeps uncover an effective bifurcation in the  $\xi, \tau_{VA}$  plane (Fig. 5): when polarization response is fast relative to mechanical timescales, CW bias is maintained; when slow, the system counterintuitively reverses to CCW despite both cells having CW intrinsic bias. The  $\tau_{VA}$  heterogeneity creates a “tilting dumbbell” where the faster-responding cell “leads” while the slower cell anchors (Fig. 4G), producing the observed 60% CW bias and faster rotation of CW versus CCW doublets.

Our model predicts homogeneous doublets should exhibit a high percentage of coherent rotation (95%) with no directional bias. Daughter HUVEC pairs — which lack developed mechanical differences—confirm this prediction: 95% of daughter doublets rotate coherently (versus only 5% exhibiting non-coherent switching), with an equal 50/50 CW/CCW split among the rotating pairs. In contrast, non-daughter (heterogeneous) pairs show 80% coherent rotation with 60% CW bias among rotating doublets (Fig. 4H). This validates that pre-existing heterogeneity, not emergent collective properties, is nec-

essary for directional bias. The finding suggests tissue-level cell-to-cell variability may be functionally utilized to generate directional information during morphogenesis.

ROCK inhibition (decreased contractility) corresponds in our model to faster  $\tau_{VA}$  and lower  $\xi$ , shifting the system toward polarization dominance. This amplifies CW bias from 60% to 74% while reducing persistent rotation from 80% to 63%, as faster velocity alignment increases sensitivity to directional perturbations (Fig. 5E). Conversely, Calyculin A (enhanced contractility) corresponds to slower  $\tau_{VA}$ , higher  $\xi$ , and critically, stronger cell-cell repulsion  $\gamma_{cc}$  — supported by increased nuclear separation in treated doublets. This multi-parameter shift crosses the bifurcation line, reversing bias to 60% CCW with 55% persistence. The model thus interprets contractility as tuning the balance between Rho-mediated actomyosin contractility and Rac-mediated protrusion, modulating polarization machinery strength relative to mechanical constraints.

Our model simplifies intrinsic bias as noise rather than explicit cytoskeletal chirality [29, 38], uses point particles neglecting cell shape [40], ignores 3D actin organization, models velocity alignment phenomenologically rather than from Rho GTPase dynamics [24, 9], assumes constant friction rather than mechanosensitive adhesions, and takes the  $\tau_{VA}$ -contractility relationship as assumed. Future models coupling polarization to cytoskeletal architecture, incorporating mechanosensitive feedback, and deriving timescales from biochemical networks would test our framework’s robustness.

Our framework parallels chiral active matter [20, 31] but with dynamic tunability. The principle that small collectives (2-4 cells) occupy a tunable regime while larger groups lock — in may represent an evolved strategy balancing exploration with stable patterning during left-right axis specification. The timescale competition we identify — between velocity alignment, confinement, and cell-cell interaction — provides a general mechanism for how cellular collectives integrate multiple mechanical cues, relevant to neural crest migration, epithelial rotation, and cancer invasion.

This work identifies minimal physical requirements for cellular chirality: intrinsic polarization bias combined with mechanical heterogeneity creates a tunable force competition. Cellular contractility emerges as a master regulator modulating relative timescales to amplify, erase, or reverse rotational bias. The validated daughter pair prediction demonstrates that chirality requires pre-existing heterogeneity, raising questions about the origins and functional roles of cell-to-cell variability in tissues during morphogenesis and left-right axis specification.

## References

- [1] J. Algorta. *How do cells decide where to go*. PhD thesis, University of British Columbia, 2025.
- [2] R. Asai, S. Sinha, V. N. Prakash, and T. Mikawa. Bilateral cellular flows display asymmetry prior to left-right organizer formation in amniote gastrulation. *Proc. Natl. Acad. Sci. U.S.A.*, 122(6):e2414860122, 2025.
- [3] Ghina Badih, Alexandre Schaeffer, Benoit Vianay, Pauline Smilovici, Laurent Blanchoin, Manuel Théry, and Laetitia Kurzawa. Contractile forces direct the chiral swirling of minimal cell collectives. *bioRxiv*, pages 2024–09, 2024.
- [4] H. C. Berg and L. Turner. Torque generated by the flagellar motor of escherichia coli. *Biophys. J.*, 65(5):2201–2216, 1993.
- [5] B. A. Camley, Y. Zhang, Y. Zhao, B. Li, E. Ben-Jacob, H. Levine, and W. J. Rappel. Polarity mechanisms such as contact inhibition of locomotion regulate persistent rotational motion of mammalian cells on micropatterns. *Proc. Natl. Acad. Sci. U.S.A.*, 111:14770–14775, 2014.
- [6] A. Cēbers. Diffusion of magnetotactic bacterium in rotating magnetic field. *J. Magn. Magn. Mater.*, 323(3):279–282, 2011.
- [7] C. W. Chan, D. Wu, K. Qiao, et al. Chiral active particles are sensitive reporters to environmental geometry. *Nat. Commun.*, 15(1406), 2024.
- [8] A. S. Chin, K. E. Worley, P. Ray, G. Kaur, J. Fan, and L. Q. Wan. Epithelial cell chirality revealed by three-dimensional spontaneous rotation. *Proc. Natl. Acad. Sci. U.S.A.*, 115(48):12188–12193, 2018.
- [9] C. Copos and A. Mogilner. A hybrid stochastic-deterministic mechanochemical model of cell polarization. *Molecular Biology of the Cell*, 31(15):1637–1649, 2020.
- [10] J.-B. Coutelis, N. González-Morales, C. Géminard, and S. Noselli. Diversity and convergence in the mechanisms establishing L/R asymmetry in metazoan. *EMBO Rep.*, 15(9):926–937, 2014.
- [11] J. Dauparas and E. Lauga. Flagellar flows around bacterial swarms. *Phys. Rev. Fluids*, 1:043202, Aug 2016.
- [12] A. Davison et al. Formin is associated with left-right asymmetry in the pond snail and the frog. *Curr. Biol.*, 26(5):654–660, 2016.
- [13] W. R. DiLuzio, L. Turner, M. Mayer, et al. Escherichia coli swim on the right-hand side. *Nature*, 435:1271–1274, 2005.

- [14] K. Erglis et al. Dynamics of magnetotactic bacteria in a rotating magnetic field. *Biophys. J.*, 93(4):1402–1412, 2007.
- [15] A. Erzberger, A. Jacobo, A. Dasgupta, and A. J. Hudspeth. Mechanochemical symmetry breaking during morphogenesis of lateral-line sensory organs. *Nat. Phys.*, 16(9):949–957, 2020.
- [16] B. M. Friedrich and F. Jülicher. Chemotaxis of sperm cells. *Proc. Natl. Acad. Sci. U.S.A.*, 104(33):13256–13261, 2007.
- [17] J. Howard. *Mechanics of Motor Proteins and the Cytoskeleton*. Oxford University Press, 2018.
- [18] M. Inaki, J. Liu, and K. Matsuno. Cell chirality: its origin and roles in left-right asymmetric development. *Philos. Trans. R. Soc. B*, 371(1710):20150403, 2016.
- [19] A. Jilkine and L. Edelstein-Keshet. A comparison of mathematical models for polarization of single eukaryotic cells in response to guided cues. *PLoS Comput. Biol.*, 7(4), 04 2011.
- [20] R. Di Leonardo, L. Angelani, D. Dell’Arciprete, G. Ruocco, V. Iebba, S. Schippa, M. P. Conte, F. Mecarini, F. De Angelis, and E. Di Fabrizio. Bacterial ratchet motors. *Proc. Natl. Acad. Sci. U.S.A.*, 107(21):9541–9545, 2010.
- [21] M. Levin. Left-right asymmetry in embryonic development: a comprehensive review. *Mech. Dev.*, 122(1):3–25, 2005.
- [22] A. Mogilner and B. Fogelson. Cytoskeletal chirality: swirling cells tell left from right. *Curr. Biol.*, 25(12):R501–R503, 2015.
- [23] S. Nonaka et al. Randomization of left-right asymmetry due to loss of nodal cilia generating leftward flow of extraembryonic fluid in mice lacking kif3b motor protein. *Cell*, 95(6):829–837, 1998.
- [24] Shuichi et al. Okada. Cdk5-dependent phosphorylation of the rho family gtpase tc10 $\alpha$  regulates insulin-stimulated glut4 translocation. *Journal of Biological Chemistry*, 283(51):35455 – 35463, 2008.
- [25] P. Ray, A. S. Chin, K. E. Worley, J. Fan, G. Kaur, M. Wu, and L. Q. Wan. Intrinsic cellular chirality regulates left-right symmetry breaking during cardiac looping. *Proc. Natl. Acad. Sci. U.S.A.*, 115(50):E11568–E11577, 2018.
- [26] I. H. Riedel, K. Kruse, and J. Howard. A self-organized vortex array of hydrodynamically entrained sperm cells. *Science*, 309(5732):300–303, 2005.
- [27] Balint Szabo, GJ Szöllösi, B Gönci, Zs Jurányi, David Selmeczi, and Tamás Vicsek. Phase transition in the collective migration of tissue cells: experiment and model. *Physical Review E—Statistical, Nonlinear, and Soft Matter Physics*, 74(6):061908, 2006.
- [28] Y. H. Tee, W. J. Goh, X. Yong, et al. Actin polymerisation and crosslinking drive left-right asymmetry in single cell and cell collectives. *Nat. Commun.*, 14(776), 2023.
- [29] Y. H. Tee, W. J. Goh, X. Yong, H. T. Ong, J. Hu, I. Y. Y. Tay, S. Shi, S. Jalal, S. F. H. Barnett, P. Kanchanawong, et al. Actin polymerisation and crosslinking drive left-right asymmetry in single cell and cell collectives. *Nat. Commun.*, 14(1):776, 2023.
- [30] Y. H. Tee, T. Shemesh, V. Thiagarajan, R. F. Hariadi, K. L. Anderson, C. Page, N. Volkmann, D. Hanein, S. Sivaramakrishnan, M. M. Kozlov, et al. Cellular chirality arising from the self-organization of the actin cytoskeleton. *Nat. Cell Biol.*, 17(4):445–457, 2015.
- [31] B. ten Hagen, F. Kümmel, R. Wittkowski, et al. Gravitaxis of asymmetric self-propelled colloidal particles. *Nat. Commun.*, 5(4829), 2014.
- [32] D. Vahabli and T. Vicsek. Emergence of synchronised rotations in dense active matter with disorder. *Commun. Phys.*, 6(56), 2023.
- [33] S. Lo Vecchio, O. Pertz, M. Szopos, L. Navoret, and D. Riveline. Spontaneous rotations in epithelia as an interplay between cell polarity and boundaries. *Nat. Phys.*, 20(2):322–331, 2024.
- [34] B.-C. Wang et al. Cell chirality regulates coherent angular motion on small circular substrates. *Biophys. J.*, 121(10):1931–1939, 2022.
- [35] W. B. Wood. Left-right asymmetry in animal development. *Annu. Rev. Cell Dev. Biol.*, 13:53–82, 1997.
- [36] S. Wu, L. Ruan, J. Wu, M. Wu, L. T. Chu, H. K. Kwong, M. L. Lam, and T.-H. Chen. Scalable pattern formation of skeletal myotubes by synergizing microtopographic cues and chiral nematics of cells. *Biofabrication*, 15(2):025015, 2023.
- [37] L. Xu, X. Wang, W. Wang, et al. Enantiomer-dependent immunological response to chiral nanoparticles. *Nature*, 601:366–373, 2022.
- [38] T. Yamamoto, T. Ishibashi, Y. Mimori-Kiyosue, S. Hiver, N. Tokushige, M. Tarama, M. Takeichi, and T. Shibata. Epithelial cell chirality emerges through the dynamic concentric pattern of actomyosin cytoskeleton. *bioRxiv*, pages 2023–08, 2023.
- [39] H. Zhang, T. Rahman, S. Lu, A. P. Adam, and L. Q. Wan. Helical vasculogenesis driven by cell chirality. *Sci. Adv.*, 10(8):eadj3582, 2024.

- [40] Falko Ziebert, Sumanth Swaminathan, and Igor S Aranson. Model for self-polarization and motility of keratocyte fragments. *Journal of The Royal Society Interface*, 9(70):1084–1092, 2012.